中國機械工程學刊第四十卷第二期第 109~118 頁(民國一百零八年)
Journal of the Chinese Society of Mechanical Engineers, Vol.40, No.2, pp 109~118 (2019)

A Novel Worm Drive via Selecting the Segments of Tooth Profile Helix

Jie Yang*and Deng-zhou Hu**

Keywords： Novel modeling method, spiral helix cocoon, tooth segments, meshing performance, prototype machine.

ABSTRACT

In order to research a new worm drive modeling design method, and achieve the purpose of simplifying design, taking the anti-backlash planar enveloping endface meshing toroidal worm drive for example, this study firstly seeks to investigate a new method of constructing the worm tooth profile helical line, according to the characteristic of the planar enveloping hourglass worm tooth profile structure, which can be formed a tooth profile helical line similar to the spiral cocoon when the varying parameter of planar external gear rotational angle c is equal to 4π , and adjusting c value to 1.2π and 0.3π respectively, the left and right end-faces tooth profile segments in the spiral cocoon can be selected to construct the bilaterally symmetric worms. Secondly, the effects of the main design parameters on the meshing performances of this novel worm drive are investigated, it is figured out except for the transverse module, the significant influence is given to improve the meshing performance by increasing inclination angle of planar external gear and radius of base circle. Lastly, the prototype machine is manufactured based on this worm forming principle, and the corresponding tests are carried out. This paper provides a new reference for the follow-up research of worm drive to a certain extent.

Paper Received January, 2018. Revised March, 2018. Accepted August, 2018. Author for Correspondence: Jie Yang

* *School of Mechanical Engineering, Xihua University, No. 999 Jinzhou road, Jin-niu district, Chengdu, Sichuan, China*

** *Department Of Aviation Manufacturing Engineering, Chengdu Aeronautic Polytechnic, No. 699 Checheng east seven road, Long quan-yi district, Chengdu, Sichuan, China*

INTRODUCTION

The toroidal worm drive is characterized with less noise, multi-tooth meshing, strong carrying capacity, compact structure, excellent lubrication performance and so on, it is widely applied in the mining machine, construction equipment, and versatile machine tool (Chen et al (2013); Simon (2015); Bair and Tsay (1999); Sandler, Lagutin et al (2014)). However, due to backlash between the conjugated meshing tooth, the failure forms such as pitting, tooth surfaces gluing and fracture are caused by the conjugated tooth surfaces impacted in frequent corotation-reversal motion, not only is the mechanism service life affected seriously, but also the transmission accuracy is reduced. So considerable research efforts had been devoted to designing structures for eliminating the backlash between the conjugated tooth pairs, such as Kacalak et al (2016) presented a kind of worm gear drive with a locally axially adaptive worm, the backlash could be eliminated or adjusted by using this specially designed worms and worm wheels. Sobolak and Jagiełowicz (2014) used the globoidal worm gear with the rotary teeth in the shape of the frustum of cone to replace the classical worm wheel for eliminating the backlash. Deng et al (2013) developed a hourglass worm gear with the symmetrically distributed double-rollers for eliminating or reducing errors. Qiu et al (2011) proposed the gradual-change tooth thickness planar worm gear, the backlash was eliminated depending on axis displacement of the worm gear. They provided the valuable experiences to design the new structure for eliminating the backlash.

This research provides a novel modeling method of worm drive, which is that the tooth profile spiral cocoon can be formed through increasing the parameter of planar external gear rotational angle c to a certain range, and the different structures of worm drives can be constructed by adjusting c in this range. Based on this theory, the corresponding tooth of the anti-backlash planar endface meshing toroidal worm drive is developed (hereinafter referred to as endface meshing toroidal worm drive).

In this paper, the novel worm drive modeling theory is based on the moving coordinate frame method, the differential geometry and the classical gear meshing theory (Qi et al (1987); Kubo (2016); Chen (1990)). Then the influences of main parameters such as the inclination angle, transverse module and radius of the base circle on the meshing performances are also investigated. The first prototype machine is manufactured and the relevant performance tests are carried out for preliminary verification in the actual working condition at last.

MATHEMATICAL MODEL

The tooth surfaces of anti-backlash planar enveloping endface meshing toroidal worm drive, which are considered as the conjugated surfaces, and they are generated by a series of enveloping external gear planar surfaces, the coordinate systems in the enveloping process can be represented, the fixed coordinate systems as $\Sigma_1(O_1, X_1, Y_1, Z_1)$ and $\Sigma_2(O_2, X_2, Y_2, Z_2)$ are respectively indicated the initial position of this endface meshing toroidal worm and planar external gear, the movable coordinate systems as $\Sigma_{1'}(O_{1'}, X_{1'}, Y_{1'}, Z_{1'})$ and $\Sigma_{2'}(O_{2'}, X_{2'}, Y_{2'}, Z_{2'})$ are respectively rigidly connected the endface meshing toroidal worm and planar external gear. The endface meshing toroidal worm and the planar external gear rotate about axes Z_1 and Z_2 with the angular velocity vectors $\omega^{(1)}$ and $\omega^{(2)}$ respectively. The rotation angles are φ_1 and φ_2 respectively. The radius of main base circle is r_b, the center distance is A, and the inclination angle of planar external gear is β, and for convenience in computation, and the coordinate systems of arbitrary meshing point O_P can be set up as $\Sigma_3(O_P, X_3, Y_3, Z_3)$ and $\Sigma_{2'}(O_{2'}, X_{2'}, Y_{2'}, Z_{2'})$. The cross angle between the axes Z_3 and $Z_{2'}$ is also equaled to β, the two perpendicular axes of $O_{2'}X_{2'}$ and $O_P X_3$ are expressed as the orthogonal parameters u and v, as shown in Fig. 1.

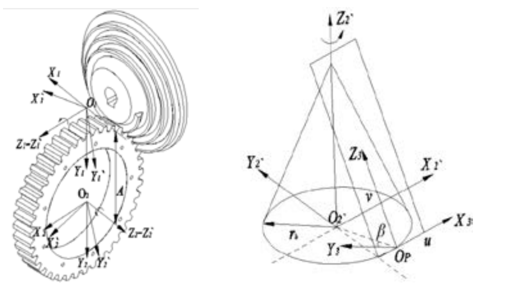

Fig. 1. The worm drive coordinate systems.

As shown in Fig. 1, the mathematical expression of the movable coordinates can be obtained by the relation of frames $\Sigma_{1'}$ and $\Sigma_{2'}$, the mathematical expression between frames $\Sigma_{2'}$ and Σ_3 are obtained respectively as following:

$\Sigma_{1'} \leftrightarrow \Sigma_{2'}$

$$\begin{bmatrix} x_{2'} \\ y_{2'} \\ z_{2'} \\ 1 \end{bmatrix} = \mathbf{M}_{2'2}\mathbf{M}_{21}\mathbf{M}_{11'} \begin{bmatrix} x_{1'} \\ y_{1'} \\ z_{1'} \\ 1 \end{bmatrix}$$

$$= \begin{bmatrix} -cos\varphi_1 cos(c\varphi_2) & cos(c\varphi_2) sin\varphi_1 & -sin(c\varphi_2) & Acos(c\varphi_2) \\ cos\varphi_1 sin(c\varphi_2) & -sin(c\varphi_2) sin\varphi_1 & -cos(c\varphi_2) & -Asin(c\varphi_2) \\ -sin\varphi_1 & -cos\varphi_1 & 0 & 0 \\ 0 & 0 & 0 & 1 \end{bmatrix} \begin{bmatrix} x_{1'} \\ y_{1'} \\ z_{1'} \\ 1 \end{bmatrix} \quad (1)$$

$\Sigma_{2'} \leftrightarrow \Sigma_3$

$$\begin{bmatrix} x_3 \\ y_3 \\ z_3 \\ 1 \end{bmatrix} = \begin{bmatrix} 1 & 0 & 0 & 0 \\ 0 & cos\beta & -sin\beta & r_b sin\beta \\ 0 & sin\beta & cos\beta & r_b cos\beta \\ 0 & 0 & 0 & 1 \end{bmatrix} \begin{bmatrix} x_{2'} \\ y_{2'} \\ z_{2'} \\ 1 \end{bmatrix} = \mathbf{M}_{32'} \begin{bmatrix} x_{2'} \\ y_{2'} \\ z_{2'} \\ 1 \end{bmatrix} \quad (2a)$$

$$\left.\begin{aligned} x_{2'} &= u \\ y_{2'} &= -r_b + v\sin\beta \\ z_{2'} &= v\cos\beta \end{aligned}\right\} \quad (2b)$$

Without loss of generality (Chen et al (2013)), this endface meshing toroidal worm rotation angular velocity is supposed as $\omega^{(1)} = 1\ rad/s$, and according to the transmission ratio, the planar external gear rotation angular velocity is $\omega^{(2)} = 1/i_{12}\ rad/s$. Thus, the expressions of relative velocity vector and angular velocity vector are expressed as following:

$$\mathbf{v}^{(21)} = \left[v_x^{(21)}, v_y^{(21)}, v_z^{(21)}\right]^T$$
$$= \left[-i_{21} + \cos(c\varphi_2), i_{21} - \sin(c\varphi_2), -\cos(c\varphi_2) + \sin(c\varphi_2) + A\right]^T \quad (3)$$

$$\boldsymbol{\omega}^{(21)} = \boldsymbol{\omega}^{(2)} - \boldsymbol{\omega}^{(1)} = \left[\omega_x^{(21)}, \omega_y^{(21)}, \omega_z^{(21)}\right]^T$$
$$= \left[\sin(c\varphi_2), \cos(c\varphi_2), i_{21}\right]^T \quad (4)$$

In combination with Fig 2, the unit normal vector of the meshing point was represented as following:

$$\mathbf{n}^{(21)} = \left[n_x\ n_y\ n_z\right]^T = \left[0\ -\cos\beta\ \sin\beta\right]^T \quad (5)$$

According to the classical gear meshing theory (Chen (1990)), the relative velocity vector $\boldsymbol{v}^{(21)}$ and unit normal vector of the meshing point $n^{(21)}$, which are in tangency during the whole conjugated meshing process. In combination with formulas (1), (2a), (2b), (3) and (5), the satisfied meshing condition equation is obtained as following:

$$\boldsymbol{\Phi}(u, v, c\varphi_2) = \mathbf{n}^{(21)} \cdot \mathbf{v}^{(21)} = 0 \quad (6)$$

According to above-mentioned analyses, the equation set of this worm tooth surface is derived after simplifying as following:

$$\left.\begin{array}{l} v=\dfrac{ui_{21}cos\beta+sin\beta\cdot\left[cos\left(c\varphi_2\right)u+r_b sin\left(c\varphi_2\right)-A\right]}{sin\left(c\varphi_2\right)} \qquad \varphi_2\neq 0 \\ x_{2'}=u \\ y_{2'}=-v\sin\beta+r_b \\ z_{2'}=v\cos\beta \\ x_{1'}=-x_{2'}cos\varphi_1cos\left(c\varphi_2\right)+y_{2'}cos\varphi_1sin\left(c\varphi_2\right)-z_{2'}sin\varphi_1+Acos\varphi_1 \\ y_{1'}=x_{2'}cos\left(c\varphi_2\right)sin\varphi_1-y_{2'}sin\left(c\varphi_2\right)sin\varphi_1-z_{2'}cos\varphi_1-Asin\varphi_1 \\ z_{1'}=-x_{2'}\sin\left(c\varphi_2\right)-y_{2'}\cos\left(c\varphi_2\right) \end{array}\right\} \qquad (7)$$

In this example, according to equation set (7), the tooth profile of ordinary planar enveloping hourglass worm is formed when c is equal to 1 as shown in Fig. 2 a), the tooth profile spiral cocoon is formed as shown in Fig. 2 b) after increasing c to 4π, it is not hard to figure out this spiral cocoon that can be divided into dual layers, the planar enveloping hourglass worm's tooth profile is belonged to the mid segment in the inner layer, and the tooth profile of bilaterally symmetric end-faces meshing toroidal worms are selected as shown in Fig. 2 c) after c is equal to 1.2π and 0.3π respectively. So in other words, the various worm drives with different functions can be designed by this method.

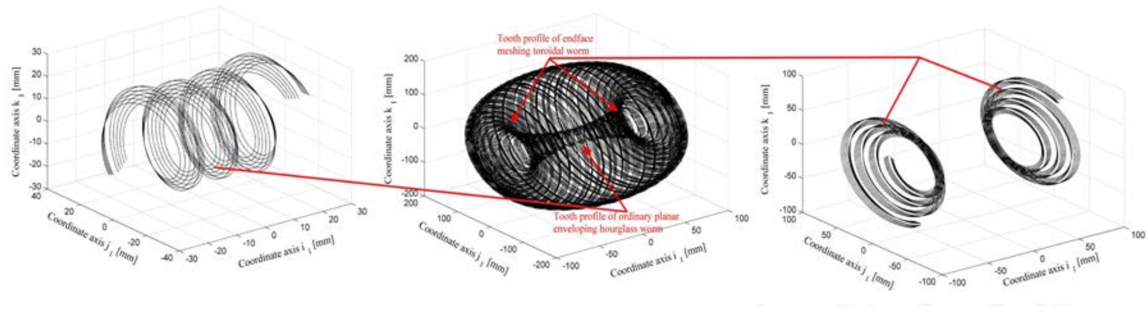

a) b) c)

Fig. 2. The shapes of the worm tooth profile spiral line with different parameter c.

Due to the backlash (Ren et al (2014); Polyakov et al (2016)), the feeding movement is delayed when the system suddenly rotates reversely, the operating accuracy of entire transmission system is reducing, and wearing on the tooth surfaces is serious under the condition of the corotation-reversal motion. In order to resolve this problem, the bilaterally symmetric end-faces worms are connected by a drive shaft as shown in Fig. 3, the working process is assumed that right worm provides power when this system rotates positively, suddenly this system runs reversely, the left worm provides power, and the part of former providing power is changed into the eliminating backlash part, the whole working process does not need any other aided components.

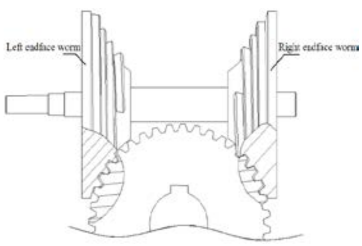

Fig. 3. The novel worm drive structure.

INFLUENCES OF MAIN DESIGN PARAMETERS ON MESHING PERFORMANCES

The meshing performances can be investigated by the meshing tooth contact area, induced principle curvature and sliding angle, the specific analyses are shown as following:

(1) Meshing tooth contact area

The meshing tooth contact area is divided into two parts by a meshing limit line, one part is the meshing area, and the other is non-meshing area, it can be figured out that the larger meshing area is, the better meshing performance and transmission efficiency are in the whole meshing process. The meshing limit function is obtained by taking partial derivation with respect to the time variable t in Eq (6), it was as following equation (8):

$$\begin{aligned}\Phi_t\left(u,v,c\varphi_2\right)&=\frac{d\,\Phi\left(u,v,c\varphi_2\right)}{d\,t}\\&=i_{21}\left[\left(v-r_bsin\beta\right)cos\left(c\varphi_2\right)+usin\beta sin\left(c\varphi_2\right)\right]=0\end{aligned} \qquad (8)$$

(2) Induced principle curvature

$k_\sigma^{(21)}$ is the induced principle curvature that describes the normal curvatures difference of arbitrary contact points on the conjugated tooth surfaces along the tangent direction, and smaller induced principle curvature reflects the conjugated tooth surfaces with higher load capacity (Deng et al (2013); Qi et al (1987)). Based on the classical gear meshing theory and moving coordinate frame method (Chen (1990); Kikuchi and Tsurumoto (1993)), $k_\sigma^{(21)}$ can be represented as following:

$$\left.\begin{aligned} & k_\sigma^{(21)} = \frac{\boldsymbol{\sigma}^2}{\psi} \\ & \boldsymbol{\sigma} = \left[\omega_{ey}{}^{(21)}, -\omega_{ex}{}^{(21)}, 0\right]^T \\ & \psi = \boldsymbol{\Phi}_{\mathbf{t}}\left(u, v, c\varphi_2\right) + \omega_{ey}{}^{(21)} v_{ex}^{(21)} - \omega_{ex}{}^{(21)} v_{ey}^{(21)} \\ & \boldsymbol{\Phi}_{\mathbf{t}}\left(u, v, c\varphi_2\right) = \frac{d\,\boldsymbol{\Phi}\left(u, v, c\varphi_2\right)}{d\,t} \end{aligned}\right\} \tag{9}$$

(3) Sliding angle

μ is defined as the sliding angle, which is the acute angle between the contact line and relative translation velocity vector, the EHL oil film is easier to be formed under the condition of the bigger sliding angle (Craig (1986)).

$$\mu = \arcsin \frac{v_{ex}^{(21)} \omega_{ey}^{(21)} - v_{ey}^{(21)} \omega_{ex}^{(21)}}{\sqrt{\left(v_{ex}^{(21)}\right)^2 + \left(v_{ey}^{(21)}\right)^2} \cdot \sqrt{\left(\omega_{ex}^{(21)}\right)^2 + \left(\omega_{ey}^{(21)}\right)^2}} \tag{10}$$

The main design parameters such as different values of planar external gear's inclination angle, transverse module and radius of base circle, not only can the structural size be decided, but meshing performances are determined, so investigating the influences of different parameters on meshing performances are necessary. Substituting values from columns A, B and C in Table 1 into Eqs (8) ~ (10), the corresponding to values of the meshing performances can be analyzed.

Table 1. Design parameters of the worm drive

Parameters	**values**		
	A	B	C
Inclination angle of planar external gear, β(°)	2	4	6
Transverse module, $m_t(mm)$	4	4.5	5
Radius of base circle, $r_b(mm)$	29	31.5	34

(1) Influence of inclination angle of planar external gear on meshing performance

For examples, three values are selected to investigate the influence of increasing the inclination angle on meshing performances.

① Influence of β on meshing area

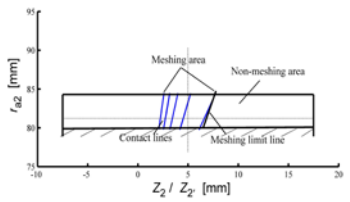

a) $\beta = 2°$

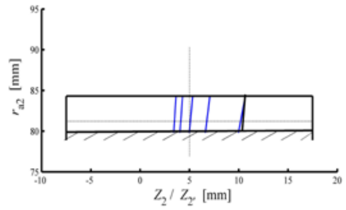

b) $\beta = 4°$

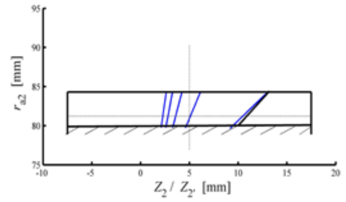

c) $\beta = 6°$

Fig. 4. The influences of β on meshing area.

It is shown in Fig.4., r_{a2} represents the arbitrary teeth addendum radius of planar external gear, and $Z_2 / Z_{2'}$ represents the projection length of the arbitrary teeth in the direction of $Z_2 / Z_{2'}$ axis.

It is not hardly found that the meshing process is enlarged by increasing the inclination angle of planar external gear. In other words, increasing β can obtain higher utilization ratio of meshing tooth surfaces, however, worm addendum pointing is caused by excessive increasing β value, so it should not be too large (Bair and Tsay (1998)).

② Influence of β on induced principle curvature distribution

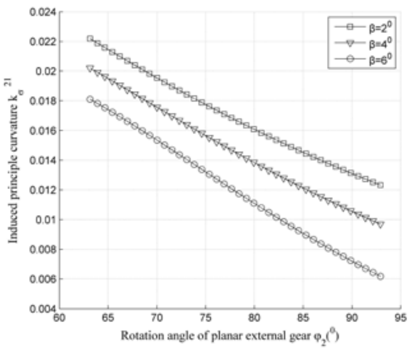

Fig. 5. The influence of β on induced principle curvature.

The distribution of the induced principle curvature is obvious reduced in the whole meshing process, and its overall trend of induced principle is reduced as raising the inclination angle of planar external gear, so it can be expressed that increasing β, the higher load capacity is obtained to a certain extent.

③ Influence of β on sliding angle distribution

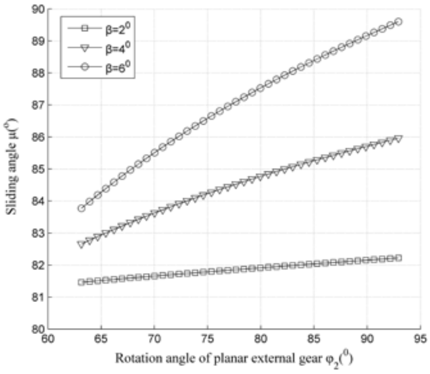

Fig. 6. The influence of β on sliding angle distribution.

From the Fig.6, the distribution of sliding angle is raised in meshing process, and the overall trend of μ, which is raised as increasing the β, it is figured that appropriate increasing β, the lubrication performance can be improved effectively.

(2) Influence of transverse module on meshing performance

Substituting the different parameters of transverse module from Table 1 into the equation (8), the results can be shown as following:

① Influence of m_t on meshing area

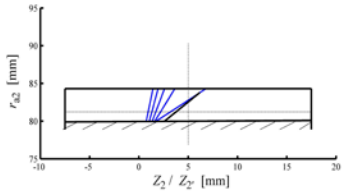

a) $m_t = 4mm$

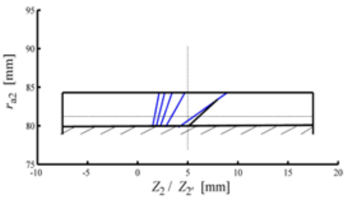

b) $m_t = 4.5mm$

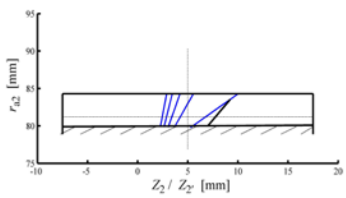

c) $m_t = 5mm$

Fig. 7. The influence of m_t on meshing area.

The formed meshing area is increased through raising transverse module, however, the extent of increment is not obvious.

② Influence of m_t on induced principle curvature distribution

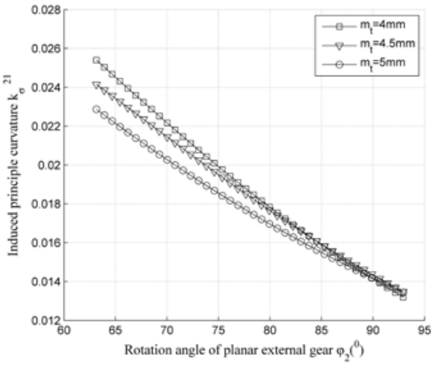

Fig. 8. The influence of m_t on induced principle curvature.

Obviously, the overall distribution of induced principle curvature is reduced in the whole meshing process, and $k_{\sigma}^{(21)}$ is also reduced through raising m_t, however, the decline amplitude is rather small.

③ Influence of m_t on sliding angle distribution

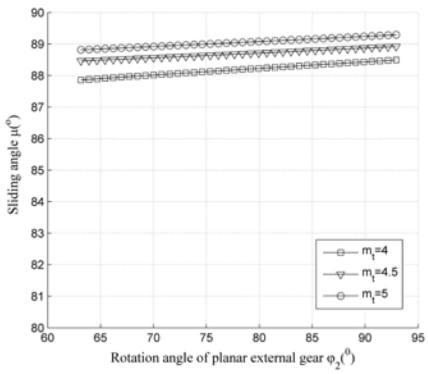

Fig. 9. The influence of m_t on sliding angle.

Apparently, the distribution of the sliding angle is raised in the whole meshing process, but raising m_t has a little effect on promoting lubrication condition, as shown in Fig. 9.

(3) Influence of radius base circle on meshing performance

The influence of the radius of base circle on the meshing performances are investigated at last, as shown in Fig. 10.

① Influence of r_b on contact lines distribution

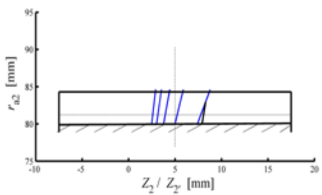

a) $r_b = 29mm$

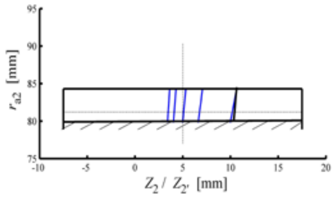

b) $r_b = 31.5mm$

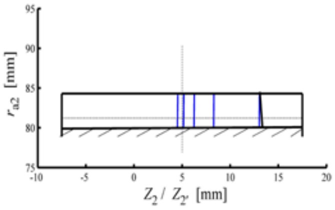

c) $r_b = 34mm$

Fig. 10. The influence of r_b on meshing area.

From the Fig. 10, it is obviously shown that the contact performance is improved by increasing r_b.

② Influence of r_b on induced principle curvature distribution

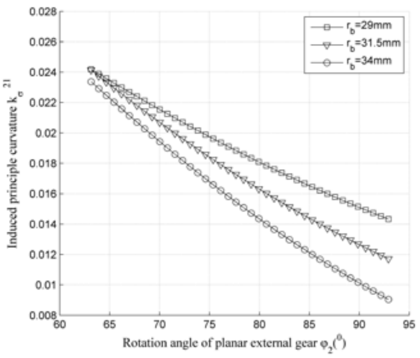

Fig. 11. The influence of r_b on induced principle curvature.

It shows that the overall distribution of induced principle curvature is reduced in the whole meshing process, and $k_\sigma^{(21)}$ is reduced effectively by raising r_b.

③ Influence of r_b on sliding angle distribution

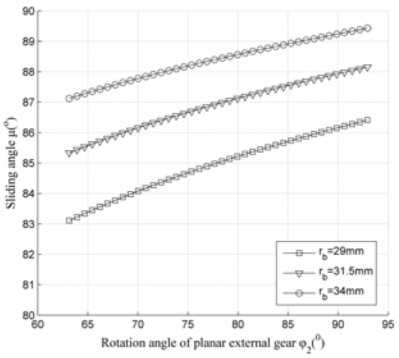

Fig. 12. The influence of r_b on sliding angle.

Apparently, the distribution of sliding angle is raised by increasing r_b, so to speak, the great effect of EHL is determined by lager r_b value.

To sum up, these results prove the meshing performances improved by proper increasing β and r_b, however, increasing m_t has little effect to the meshing performances.

PROTOTYPE MACHINING AND PERFORMANCE TESTS

According to the moving coordinate frame method and rigid body motion theory (Chen et al (2013); Qi (1987)), the relative movement of the knife tool and novel worm can be expressed as following:

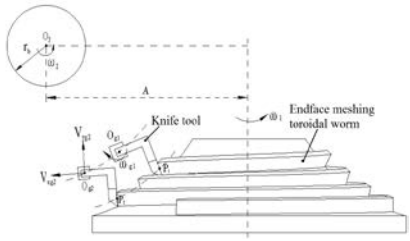

Fig. 13. The relationship of relative movement.

The angular velocity ω_1 of this worm can be shown, O_{g1} and O_{g2} are respectively expressed as the rotational axis of knife tool at arbitrary time, P_1 and P_2 are the contact points of the knife tool and worm at different moments, the rotational motion of knife tool rotates about axis O_2 with the angular velocity ω_2, which can be decomposed into two direction-motions, one is the knife tool that is rotating about axis O_{g1}, and the other is the knife tool translation motion along the arc $O_{g1}O_{g2}$, so the kinematics relation equations can be set up as following:

$$\left.\begin{aligned} &\omega_2 \times r_{O_2P_2} = \left(v_{xg2} + v_{yg2}\right) + \omega_{g2} \times r_{O_{g2}P_2} \\ &\omega_{g2} = \omega_{g1} = \omega_2 \\ &v_{xg2} + v_{yg2} = \omega_2 \times r_{O_2O_{g2}} \end{aligned}\right\} \tag{11}$$

According to above analyses, the prototype model of this novel worm drive can be constructed, as shown in Fig. 14:

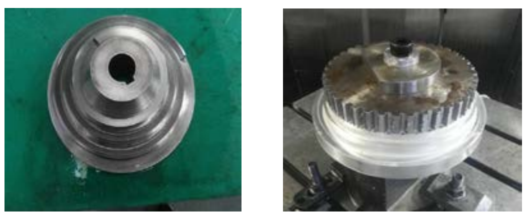

a) worm b) worm gear

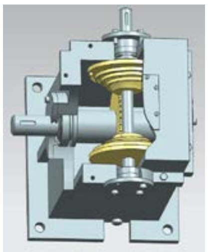

c) 3D prototype diagram

Fig. 14. The prototype model.

The worm drive test platform is installed for investigating this prototype machine performances, the equipments are linked by pin-disk coupling, the input and output powers can be measured by each torque and rotating speed sensor, the reductor is installed between the prototype machine and loading motor, which plays the role in adjusting rotational speed and torque, the layout of this test platform is shown in Fig. 15.

Fig. 15. The test platform layout.

Table 2. Components of the test platform

Serial numbers	Mechanical components
①	Main control panel
②	Motor Control cabinet
③	Loading motor
④	Reductor
⑤	Pin-disk couplings ,torque and rotational speed transducers
⑥	Prototype machine
⑦	Driving motor

To test the meshing performance under the condition of positive and reverse rotation, the method is daubing the sudan red on the worm tooth surfaces, and driving this worm positive and reverse running, it can be figured out form Fig. 16, the sudan red is spread evenly on the gear's tooth surfaces. This test demonstrates that this structure's meshing performance is well.

a) positive operation b) reverse operation

Fig. 16. The corotation-reversal operations.

To test the transmission efficiency and temperature rising of this worm drive when it is positive and reverse running, the method is that the input rotational speed is gradually raised from 0 to $1000rpm$, and the output torque is also slowly increased from 0 to $800N \cdot m$, the values of the oil temperature and transmission efficiency are measured, and these tests respectively last 2 hours. The results show that the oil temperature-risings are respective $88.4°C$ and $89.2°C$, and the transmission efficiencies are respective 61.3% and 62.7% when input rotational speed and the output torque are closed to $1000rpm$ and $800N \cdot m$ under the circumstance of the motor positive and reverse running, however, the high noises on this prototype machine and massive white smoke from the thermovent due to continuing to increase the input rotational speed and output torque, and it is found that the worm tooth surfaces are with varying degrees of wears after running stopped, as shown in Fig. 17.

Fig. 17. The situation of the wear on the worm tooth surfaces.

CONCLUSIONS

Proposed is a novel endface meshing toroidal worm drive modelling method, based on above researches, the following conclusions can be summarized:

(1) According to the characteristic of the planar enveloping hourglass worm drive, which is that the structure of tooth profile can be obtained by adjusting the varying parameter of the planar external gear rotation angle without changing the other design parameters and the complex mathematical deductions, based on this design method, the anti-backlash planar endface

meshing toroidal worm drive is developed.

(2) To research the effects of the main design parameters on the meshing performances, by careful theoretical derivations and calculations, the results show that in addition to increment the transverse module, the meshing performances are improved by increasing inclination angle of planar external gear and the radius of base circle to a certain extent.

(3) The prototype machine is manufactured according to the moving coordinate frame method and rigid body motion theory, and the performance tests are carried out, the results show that the meshing performance of this prototype machine is well, the oil temperature-risings are respective $88.4°C$ and $89.2°C$, and the transmission efficiencies are respective 61.3% and 62.7% under the condition of the motor positive and reverse running, however, keeping increasing the input rotational speed and output torque, the different degrees of wears occur on the worm tooth surfaces. In further study, the experimental methods of eliminating the backlash and error analysis should be designed to verify the anti-backlash function of this novel worm drive.

ACKNOWLEGEMENT

The prototype machine manufacturing and performance tests in this paper were respectively supported by Department Of Aviation Manufacturing Engineering, Chengdu Aeronautic Polytechnic and School of Mechanical Engineering, Xihua University, this research fund was provided by the Spring plan of China's Ministry of Education under grant No. 14202505.

REFERENCES

Chen, Y, H., Zhang, G, H., Chen, B, K., Luo W, J., Li, F, J., Chen, Y., "A novel enveloping worm pair via employing the conjugating planar internal gear as counterpart," MECH MACH THEORY, Vol. 67, No. 9, pp. 17-23 (2013).

Simon, V, V., "Influence of tooth errors and shaft misalignments on loaded tooth contact in cylindrical worm gears," MECH MACH THEORY, Vol. 41, No. 6, pp. 707-724 (2015).

Bair, B, W., Tsay, C, B., "Sensitivity Analysis and Surface-Deviation Minimization of ZK-Type Dual-Lead Worm Gear Drives," J MECH DESIGN, Vol. 121, No. 3, pp. 409-415 (1999).

Sandler, A, I., Lagutin, S, A., Gudov, E, A., "Longitudinal contact localization in worm gears," Russian Engineering Research, Vol. 34, No. 7, pp. 480-486 (2014).

Kacalak, W., Majewski, M., Budniak, Z., "Worm Gear Drives With Adjustable Backlash." J MECH ROBOT, Vol. 8, No. 1, pp. 014504 (2016).

Sobolak, M., Jagiełowicz, P., "The Globoidal worm gear with rotary teeth and autodenous backlash self-eliminating used in motorization,"Journal of Kones, Vol. 21, No. 1, pp. 267-272 (2014).

Deng, X, Q., Wang, J, G., Horstemeyer, M, F., "Modification Design Method for an Enveloping Hourglass Worm Gear with Consideration of Machining and Misalignment Errors," CHIN J MECH ENG-EN, Vol. 26, No. 5, pp. 948-956 (2013).

Qiu, X, Y., Qin, D, T., Zhang, G, H., "Research on Trial-manufacture of Steel-steel Gradual-change Tooth Thickness Planar Worm Gear Drive," Journal of Sichuan University (Enginerring Science Edition), Vol. 43, No. 2, pp. 222-227 (2011).

Qi, L., Zhang, Y, X., Hu, S, C., "Worm Drive Design (2)," Peking, China, (1987).

Kubo, A., "Cause of Failure Beyond Conjugate Theory of Gear Meshing," Theory and Practice of Gearing and Transmissions. Switerland, (2016).

Chen, W, H., "Preliminary Differential Geometry," Peking, China, (1990).

Hu, L, S., Cao, H, J., Li, X, C., Zhang, C, L., Li, Y, X., "Mathematical model and geometrical model of double pitch ZN-type worm gear set based on generation mechanism," CHIN J MECH ENG-EN, Vol. 28, No. 3, pp. 549-555 (2015).

Ren, H, P., He, B., "Anti-backlash control of machine tool feed system driven by dual-motors," Electric Machines and Control, Vol. 18, No. 3, pp. 60-66 (2014).

Polyakov, S, A., Goncharov, S, Y., Kuksenova, L, I., "Development of method for evaluating performance of worm gears via analysis of their tribological characteristics," Journal of Machinery Manufacture and Reliability, Vol. 45, No. 5, pp. 458-463 (2016).

Kikuchi, S., Tsurumoto, K., "Design and characteristics of a new magnetic worm gear using permanent magne," IEEE T MAGN, Vol. 29, No. 6, pp. 2923-2925 (1993).

Craig, J, J., "Introduction to Robotics: Mechanics and Control. Massachusetts," Americ, (1986).

Bair, B, W., Tsay, C, B., "ZK-type dual-lead worm and worm gear drives : Contact teeth, contact ratios and kinematic errors," J MECH DESIGN, Vol. 120, No. 3, pp. 422-428 (1998).

NOMENCLATURE

A Center distance of the worm drive [mm]

b Width of the gear teeth [mm]

l Effective length of endface meshing toroidal worm [mm]

c Varying parameter of the planar external gear rotation angle

Z_1/Z_2 Number of the endface meshing toroidal worm thread and the planar external gear tooth, respectively

i_{12} Transmission ratio, here is Z_1/Z_2

m_t Transverse module [mm]

r_b Radius of base circle [mm]

r_{a1} Radius of worm addendum [mm]

r_{f1} Radius of worm dedendum [mm]

r_{a2} Radius of planar external gear addendum [mm]

r_{f2} Radius of planar external gear dedendum [mm]

β Inclination angle of planar external gear [°]

Σ_1, Σ_2 Fixed coordinate systems, respectively

$\Sigma_{1'}, \Sigma_{2'}$ Movable coordinate systems, respectively

Σ_3 Auxiliary coordinate system

Σ_p Coordinate system of planar external gear meshing point

$v_0^{(1)}, v_0^{(2)}$ Translational velocity vectors of movable coordinate systems origin, respectively [mm/s]

$\omega^{(1)}, \omega^{(2)}$ Angular velocity vectors of movable coordinate systems origin, respectively [rad/s]

$v^{(21)}$ Relative translation velocity vector of worm drive at the meshing point [mm/s]

$\omega^{(21)}$ Relative angular velocity vector of worm drive at the meshing point [rad/s]

φ_1, φ_2 Worm rotation angle and planar external gear rotation angle, respectively [°]

(x_n, y_n, z_n) Coordinate point value of endface meshing toroidal worm and the planar external gear in frame Σ_n, respectively $(n = 1, 2, 1', 2', 3)$

$v_x^{(21)}, v_y^{(21)}, v_z^{(21)}$ Component of $v^{(21)}$ projecting on the movable frame $\Sigma_{2'}$, respectively [mm/s]

$v_{ex}^{(21)}, v_{ey}^{(21)}, v_{ez}^{(21)}$ Component of $v^{(21)}$ projecting on the frame Σ_P, respectively [mm/s]

$\omega_{ex}^{(21)}, \omega_{ey}^{(21)}, \omega_{ez}^{(21)}$ Component of $\omega^{(21)}$ projecting on the frame Σ_P, respectively [rad/s]

M_{mn} Matrix for coordinate transformation from the frame Σ_m to Σ_n, $(m, n = 1, 2, 1', 2', 3)$

u, v Curved surface of gear parameters, respectively

φ_0 Initial meshing angle [°]

φ_w Working semi-angle [°]

Σ_p Coordinate system of planar external gear meshing point

$n^{(21)}$ Normal vector at the conjugate tooth profile of meshing point

Φ Meshing function

Φ_t Function of meshing limit

$\Psi_{(1)}$ Function of undercutting limit

φ_{2n} Planar external gear rotational angle after parameter changed [°]

$k_{\sigma}^{(21)}$ Induced principal curvature [mm^{-1}]

μ lubrication angle [°]

一種通過選擇齒廓螺旋線段的新型蝸桿傳動

楊捷
西華大學機械工程學院

胡登洲
成都航空職業技術學院航空製造系

摘 要

為了研究一種新的蝸桿傳動建模設計方法，以達到簡化設計的目的，以無側隙平面包絡端面嚙合環面蝸桿傳動為例，本研究首先探索一種新的蝸桿齒廓螺旋線的構造方法，根據平面包絡環面蝸桿齒廓結構特征，當平面外齒輪轉角C等於4π時，可形成與螺旋繭相似的齒廓螺旋線，並且將C值分別調整至1.2π和0.3π時，可以選擇螺旋繭中的左右端面齒廓構造雙側對稱的蝸桿。其次，研究了主要設計參數對該新型蝸桿傳動嚙合性能的影響，研究發現，除端面模數外，增加平面外齒輪傾角和主基圓半徑，對提高其嚙合性能有顯著的影響。最後，基於該蝸桿的成型原理製作了樣機，并進行了相應的實驗。本文在一定程度上為蝸桿傳動的後續研究提供了新的參考。